EYE DISEASE

Gene dosage manipulation alleviates manifestations of hereditary *PAX6* haploinsufficiency in mice

Behnam Rabiee[1], Khandaker N. Anwar[1], Xiang Shen[1], Ilham Putra[1], Mingna Liu[2], Rebecca Jung[1], Neda Afsharkhamseh[1], Mark I. Rosenblatt[1], Gerald A. Fishman[1,3], Xiaorong Liu[2], Mahmood Ghassemi[1], Ali R. Djalilian[1]*

In autosomal dominant conditions with haploinsufficiency, a single functional allele cannot maintain sufficient dosage for normal function. We hypothesized that pharmacologic induction of the wild-type allele could lead to gene dosage compensation and mitigation of the disease manifestations. The paired box 6 (*PAX6*) gene is crucial in tissue development and maintenance particularly in eye, brain, and pancreas. Aniridia is a panocular condition with impaired eye development and limited vision due to *PAX6* haploinsufficiency. To test our hypothesis, we performed a chemical screen and found mitogen-activated protein kinase kinase (MEK) inhibitors to induce *PAX6* expression in normal and mutant corneal cells. Treatment of newborn *Pax6*-deficient mice (*Pax6*$^{Sey\text{-}Neu/+}$) with topical or systemic MEK inhibitor PD0325901 led to increased corneal PAX6 expression, improved corneal morphology, reduced corneal opacity, and enhanced ocular function. These results suggest that induction of the wild-type allele by drug repurposing is a potential therapeutic strategy for haploinsufficiencies, which is not limited to specific mutations.

INTRODUCTION

The paired box 6 (*PAX6*) gene is a crucial transcription factor in early development and maintenance of several tissues, including the eye, brain, and pancreas (*1*). Whereas total deletion of *PAX6* results in arrested development of the eye, olfactory bulb, and brain cortex and is incompatible with life, haploinsufficiency of *PAX6* caused by mutations or deletions in one allele leads to congenital aniridia (*2*, *3*). Aniridia is a panocular condition with substantial visual impairment that can also be associated with brain, olfactory, and pancreatic abnormalities (*4*). Although iris hypoplasia is the most obvious clinical feature of aniridia, the main underlying reasons for the visual defects are foveal hypoplasia, progressive corneal opacification, cataract, and glaucoma (*5*). Whereas many of these abnormalities begin in utero and are present at birth, some develop and/or continue to progress in severity later in life (*6*). In addition to these ocular manifestations, reduced expression of *PAX6* has been associated with systemic abnormalities, including β cell failure and α cell dysfunction in diabetes, as well as several neuronal developmental conditions, such as autism (*7*, *8*).

The *PAX6* gene is a master regulator of eye and brain development in utero; however, it also plays an important role postembryonically both during early postnatal development and in adult tissue maintenance. In the eye, *PAX6* continues to be expressed in the adult retina, lens, and cornea and is essential for their function (*9*). For instance, in the corneal epithelium, it has been shown to promote differentiation, modulate cell-to-cell adhesion, and limit proliferation (*10*–*12*). Similarly, *PAX6* also plays a major role in the postnatal maintenance and function of pancreatic tissue, olfactory system, and nervous system (*13*, *14*).

More than 660 human diseases are known to result from gene haploinsufficiencies, including *PAX6*-related aniridia (*15*). In aniridic patients with a mutant *PAX6* allele, insufficient amount of PAX6 protein is responsible for the aforementioned ocular and systemic abnormalities, and the severity of the phenotype is directly correlated with *PAX6* gene dosage (*16*). Thus, increasing the expression of *PAX6* can potentially limit the development and/or progression of the congenital defects (*5*, *17*). Recently, several approaches have been reported to address haploinsufficiency, including gene replacement using a viral vector as well as genetic sequence correction and promoter activation using CRISPR (*15*, *18*). Pharmacologic enhancement of the function of the normal copy of the gene provides another approach to restore gene dosage, leading to rescue or mitigation of abnormal phenotypes (*19*). We hypothesized that using a drug repurposing strategy, it may be possible to stimulate the normal copy of *PAX6* and thus compensate for the deficiency and prevent or reduce further progression of aniridia manifestations. We tested this hypothesis in vitro on normal and mutant corneal cells and in a representative mouse model of *PAX6*-deficient aniridia (*Pax6*$^{Sey\text{-}Neu/+}$) (*20*).

RESULTS

MEK inhibition increases PAX6 expression in corneal cells

On the basis of published reports, we identified pathways that could potentially regulate *PAX6* expression and performed a targeted chemical screen of compounds that modulate these pathways. Previous studies have shown that mitogen-activated protein kinase kinase (MEK) inhibitors can indirectly increase *PAX6* expression by affecting the associated inhibitory pathways (*21*, *22*). In line with these, we found that MEK inhibitors induce *PAX6* expression in both normal and *PAX6*-deficient corneal cells (Fig. 1). On the basis of these results, PD0325901, a small molecule (molecular weight, 482.2) and a potent MEK inhibitor (K_d for MEK1, 0.4 nM in the presence and 31 nM in the absence of adenosine 5′-triphosphate), was chosen (*23*). Treatment of human corneal epithelial cells with 1 μM

[1]Department of Ophthalmology and Visual Sciences, University of Illinois at Chicago, Chicago, IL 60612, USA. [2]Departments of Biology and Psychology, University of Virginia, Charlottesville, VA 22903, USA. [3]Pangere Center for Inherited Retinal Diseases, The Chicago Lighthouse, Chicago, IL 60608, USA.
*Corresponding author. Email: adjalili@uic.edu

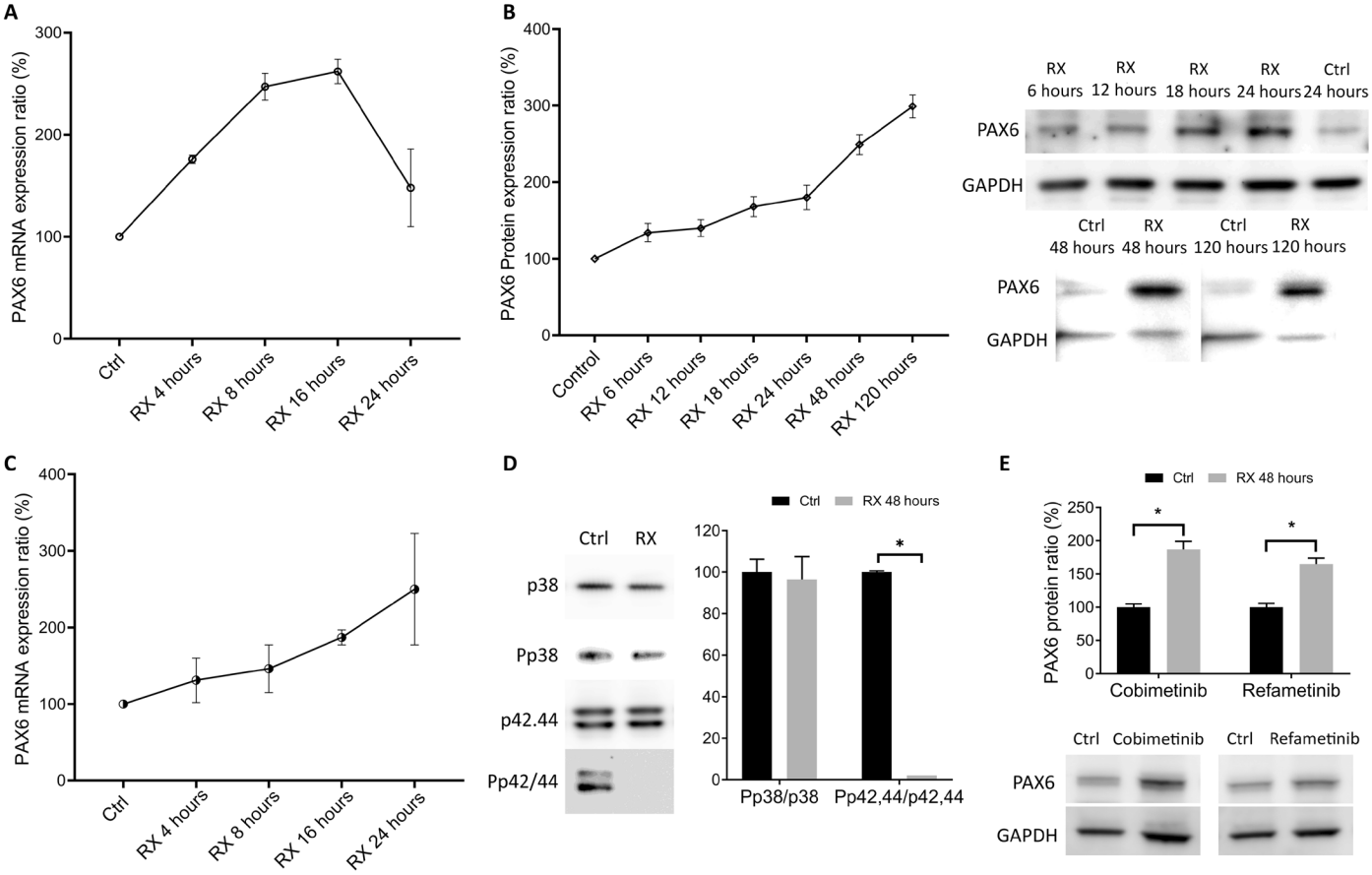

Fig. 1. The effect of MEK inhibition on *PAX6*/PAX6 expression. (**A**) *PAX6* mRNA measurement and (**B**) PAX6 protein measurement in human corneal epithelial cells treated with PD0325901 ($n = 3$). (**C**) *PAX6* mRNA measurement in murine PAX6 heterozygote corneal MSCs treated with PD0325901 ($n = 3$). GAPDH, glyceraldehyde-3-phosphate dehydrogenase. (**D**) ERK1/ERK2 inhibition measurement in human corneal epithelial cells treated with PD0325901 ($n = 3$). (**E**) PAX6 protein measurement in human corneal epithelial cells treated with two other MEK inhibitors, cobimetinib and refametinib ($n = 3$). Significance determined by *t* test. *$P < 0.05$. Ctrl, control; RX, treatment.

PD0325901 led to a significant increase in *PAX6* mRNA expression (up to 2.7 ± 0.2-fold, $P < 0.05$, $n = 3$), with a peak effect around 12 to 18 hours (Fig. 1A). Continuous treatment of human corneal epithelial cells up to 5 days likewise demonstrated a significant increase in PAX6 protein expression (up to 3.0 ± 0.3-fold, $P < 0.05$, $n = 3$) (Fig. 1B). To assess the effect of MEK inhibition on *PAX6*-deficient cells, corneal mesenchymal stromal cells isolated from $Pax6^{Sey\text{-}Neu/+}$ mice were used. Treatment with PD0325901 significantly increased *PAX6* mRNA expression in the *PAX6*-deficient corneal cells (up to 2.5 ± 0.7-fold, $P < 0.05$, $n = 3$) (Fig. 1C).

Western blot analysis of human corneal epithelial cells confirmed that this MEK inhibitor effectively and specifically suppresses extracellular signal–regulated kinase 1 (ERK1) and ERK2, while having minimal effect on p38 as the control (Fig. 1D). To confirm that the increase in *PAX6* expression is related to MEK inhibition, two other well-known MEK inhibitors—cobimetinib 1 μM and refametinib 1 μM (*24*)—were tested on human corneal epithelial cells, both of which led to increased PAX6 protein expression (cobimetinib, 1.9 ± 0.1-fold; refametinib, 1.7 ± 0.1-fold) (Fig. 1E).

Early postnatal MEK inhibition promotes a normal corneal phenotype in $PAX6^{+/-}$ mice

To assess the effects of MEK inhibition in vivo, we tested oral and topical ophthalmic application separately in a mouse model of *PAX6*-deficient aniridia ($Pax6^{Sey\text{-}Neu/+}$). On the basis of pilot studies (fig. S1), the treatment was started on postnatal day 5 (P5) (before eye opening) and continued until P30. Although the palpebral fissure is still closed with a thin membrane at P5, in the presence of dimethylsulfoxide (DMSO) in the vehicle, the drug is expected to penetrate and reach the ocular tissues (*25*).

At P30, the eyes underwent slit lamp photography and anterior segment optical coherence tomography (OCT) in vivo, followed by histologic examination (Fig. 2, A to D). It is known that in *PAX6*-deficient aniridia, corneal epithelial thickness is abnormally low, whereas corneal stromal thickness is abnormally high (*26*). Corneal epithelial thickness at P30 was significantly greater than vehicle control after both oral (26.8 ± 3.0 μm versus 16.0 ± 2.5 μm, $P < 0.001$, $n \geq 6$) and topical (26.9 ± 3.9 μm versus 14.1 ± 1.4 μm, $P < 0.0001$, $n \geq 6$) administration, indicating a phenotype closer to normal (wild type, 50.5 ± 1.1 μm, $n = 6$) (Fig. 2E), although still reduced. Furthermore, corneal stromal thickness at P30 was significantly less than vehicle control in both oral (97.7 ± 12.8 μm versus 151.8 ± 12.5 μm, $P < 0.001$, $n \geq 6$) and topical (94.4 ± 14.5 μm versus 147.8 ± 26.2 μm, $P < 0.001$, $n = 6$) treatment groups, consistent with a more normal phenotype (wild type, 75.8 ± 3.6 μm, $n \geq 6$) (Fig. 2F). Histological examination of the eyes confirmed the OCT quantifications (Fig. 2, C and D). To assess any possible adverse effects of MEK inhibition, wild-type mice were also treated postnatally

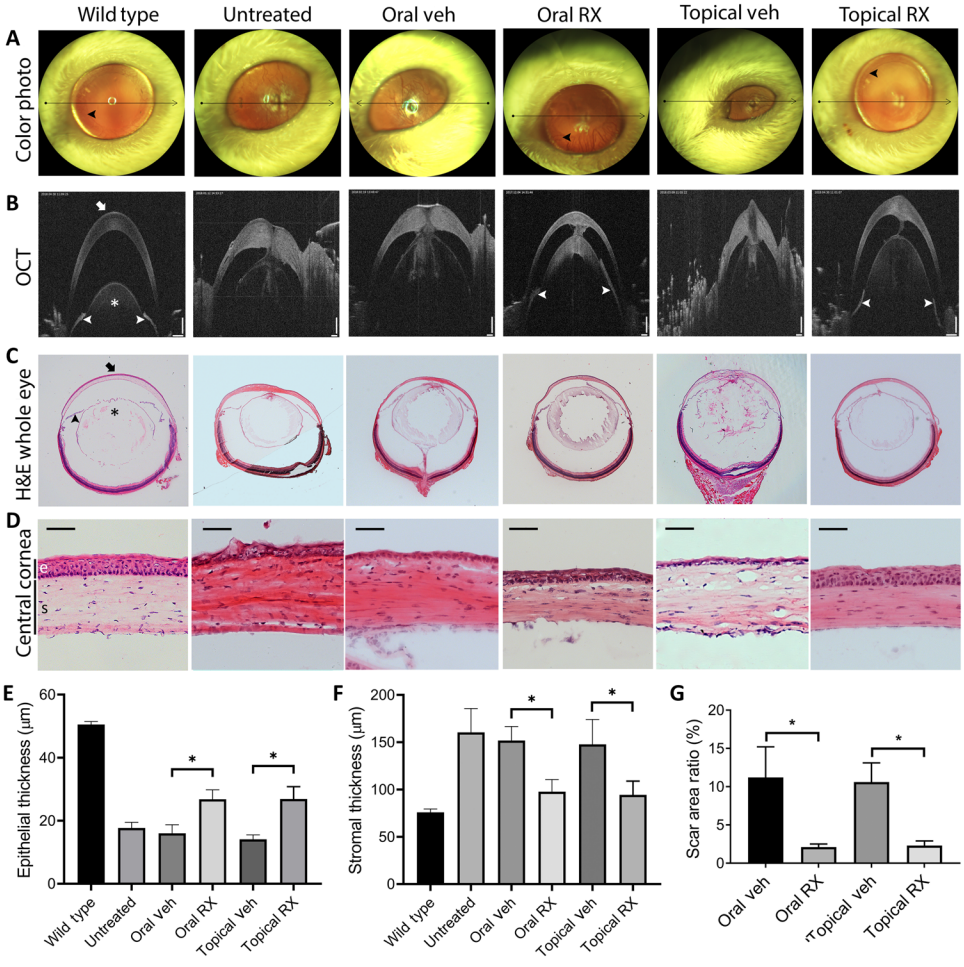

Fig. 2. P30 evaluation of *Pax6*$^{Sey\text{-}Neu/+}$ mice treated with MEK inhibitor. (**A**) Color photo, (**B**) optical coherence tomography (OCT), (**C** and **D**) hematoxylin and eosin (H&E) staining, (**E**) epithelial thickness, (**F**) stromal thickness, and (**G**) scarring ratio of mice eyes treated with systemic or topical PD0325901 ($n = 6$). The thickness measurements were done in the central cornea immediately outside the scar area (the lines in the color photos do not necessary indicate with the area of measurement). Scale bars, 50 μm. Significance determined by *t* test. *$P < 0.05$. Ctrl, vehicle control; RX, treatment. Arrow, central cornea. Asterisk, lens. Arrowhead, iris. e, epithelium; s, stroma.

(P5 to P30) with oral or topical formulations, neither of which showed any abnormalities on slit lamp exam, OCT imaging, and histologic examination (epithelial and stromal thickness in untreated wild type, 50.2 ± 0.4 and 79.3 ± 0.8; wild type with topical treatment, 50.3 ± 0.5 and 79.7 ± 0.5; wild type with oral treatment, 49.8 ± 1.2 and 78.3 ± 1.5; $P > 0.5$ for both measures, $n = 6$; fig. S2).

In the *Pax6*$^{Sey\text{-}Neu/+}$ mouse model of aniridia, the disease is typically more severe than in humans, and the eyes frequently have lens-cornea adhesions (similar to a condition known as Peter's anomaly), which are also occasionally present in the human disease (*20*). Corneal opacity (representing adhesions) was significantly less than vehicle control in both oral (scar area ratio, 2.1 ± 0.4% versus 11.2 ± 4.0%, $P < 0.001$, $n \geq 6$) and topical treatment (scar area ratio, 2.3 ± 0.6% versus 10.6 ± 2.5%, $P < 0.001$, $n \geq 6$) groups (Fig. 2G). To assess the stability of the treatment effects, the mice were examined at P60 (30 days after finishing the treatment) for corneal epithelial and stromal thickness. Corneal epithelial thickness at P60 was significantly greater than vehicle control after both oral and topical administration, indicating a phenotype closer to normal (*t* test, $P < 0.01$ for both comparisons; fig. S3, A and B). The difference in the corneal stromal thickness at P60 was only significant in the topical group (fig. S3, A and C; *t* test, $P < 0.01$). These results suggest that the effect of treatment (oral or topical) is more persistent on the epithelial phenotype and less so in terms of the stromal thickness.

It is known that in *PAX6*-deficient aniridia, corneal epithelial PAX6 protein expression is lower due to mutation/deletion in one *PAX6* allele (*5*, *17*). PAX6 immunostaining at P30 demonstrated increased PAX6 protein expression in the cornea with topical formulation compared to vehicle control (wild-type PAX6 intensity, 100%; topical treatment, 92 ± 12% versus topical vehicle, 32 ± 1%; $P < 0.01$, $n = 5$) (Fig. 3, A and C). This confirms that treatment with MEK inhibitor promoted the expression of *PAX6* in the cornea and suggests that the observed in vivo effects could be attributed to increased PAX6.

One of the most important corneal complications of *PAX6*-deficient aniridia is progressive loss of the corneal (limbal) epithelial stem cells with secondary growth of conjunctival epithelium over the cornea, leading to corneal neovascularization and scarring (*27*, *28*). To assess the effect of treatments on corneal epithelial differentiation, and the persistence of the treatment effects, immunostaining with the corneal specific cytokeratin 12 (CK12) was performed at P30 and P90. P30 CK12 immunostaining showed a more normal staining pattern in the topical treatment group compared to vehicle control, indicating improved corneal epithelial differentiation (wild-type CK12 intensity, 100%; topical treatment, 68 ± 5% versus topical vehicle, not detectable, $n = 5$) (Fig. 3, B and D).

Consistent with the P30 results, P90 CK12 immunostaining of corneal whole mounts showed a more normal pattern of staining in the topical treatment group compared to vehicle control (wild-type CK12 intensity, 100%; topical treatment, 69 ± 3% versus topical vehicle, 34 ± 1%, $P < 0.05$, $n = 5$) (Fig. 3, E and F). Overall, the favorable differentiation and preservation of the effects 60 days after stopping the treatment indicate that MEK inhibition may limit the progressive loss of limbal stem cells, while promoting their function in maintaining a normally differentiated epithelium. Given that topical treatment led to more persistent results, for the remainder of the studies, only topical treatment was evaluated.

Another important finding in aniridia is an abnormally hyperproliferative corneal epithelium (*21*). To assess the effect of treatment on corneal epithelial proliferation, Ki67 immunostaining was performed at P30. As predicted, mutant mice had significantly higher expression of Ki67 and that topical MEK inhibition resulted

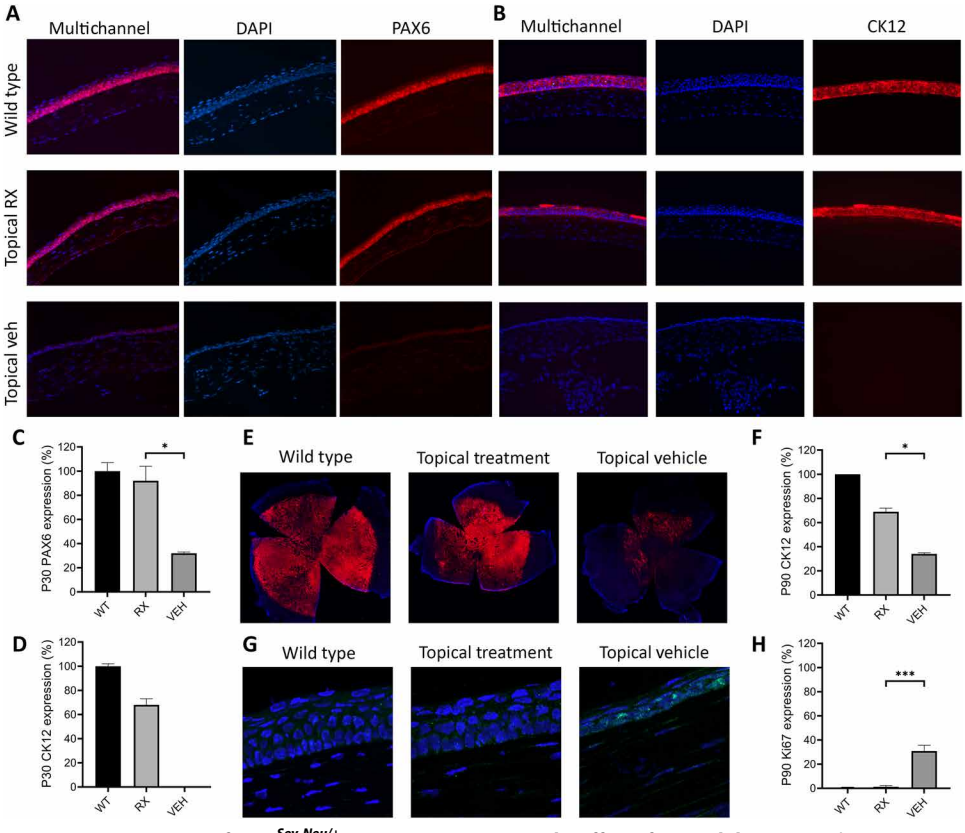

Fig. 3. Immunostaining of *Pax6*$^{Sey\text{-}Neu/+}$ mice corneas to assess the effect of MEK inhibitor. (**A** and **C**) Comparing PAX6 and (**B** and **D**) cytokeratin 12 (CK12) expression in mice corneal epithelium of the mice treated with topical MEK inhibitor with topical vehicle control on P30. Wild-type cornea immunostaining used as a reference. (**E** and **F**) CK12 immunostaining of corneal whole mount at P90. Blue, DAPI. Red, CK12. (**G** and **H**) Ki67 (proliferation marker) immunostaining of mice corneas on P30. Blue, DAPI. Green, Ki67. *$P < 0.05$ and ***$P < 0.001$. RX, MEK inhibitor treatment. Veh, vehicle control.

in significantly less proliferating cells in the corneal epithelium (1.3 ± 1.0%) compared to vehicle control (30.9 ± 4.7%, $P < 0.001$) (Fig. 3, G and H). The pattern after MEK inhibition was more similar to wild type (0.4 ± 0.6%). These results, along with the earlier findings, are consistent with the notion that hyperproliferation may be important to the corneal pathology (*21*), given that MEK inhibition, which limits proliferation, resulted in increased PAX6 and CK12 expression with concomitant reduction in Ki67.

Topical MEK inhibition promotes ocular growth and function in postnatal PAX6$^{+/-}$ mice

The mouse model of aniridia used in this study (*Pax6*$^{Sey\text{-}Neu/+}$) is also known as a small eye mouse model. To assess the effect of treatment on another manifestation of the disease in this model, we evaluated the ocular size of the treated mice versus vehicle control. At P90, treated mice eyes had significantly longer axial length compared to control (3.07 ± 0.03 versus 2.68 ± 0.31 mm, respectively; $P < 0.05$, $n = 5$), thus promoting a more normal ocular size (wild type, 3.54 ± 0.01 mm), although still reduced compared to wild type ($P < 0.5$) (fig. S4).

It has been shown that in the mouse model of aniridia, there is a substantial reduction in retinal function (*5*, *17*). This could be due to corneal defects, or functional abnormalities in the retinal photoreceptors per se (*5*, *17*). To assess the effect of treatment on retinal function, we conducted electroretinography (ERG) on the mice eyes at P90 (60 days after stopping the treatment). The amplitude of scotopic a and b waves as well as photopic b waves was significantly increased in the topical treatment group compared to vehicle control ($P < 0.05$, $n = 6$), demonstrating improvement of the retinal function in both rods and cones (Fig. 4, A to D). Furthermore, the vehicle group showed significantly delayed scotopic a and b waves, as well as photopic b wave compared to the treatment group, which showed a pattern more similar to the wild-type controls (Fig. 4, A and E to G). The observed beneficial effects on retinal function up to 60 days after stopping the treatment provide further evidence for the maintenance of the treatment effects.

To examine the effect of treatment on visual function, an optomotor response test was performed at 90 days after treatment. This test is based on the optokinetic response, which is used to measure visual function clinically in infants and experimentally in animal models (*29*, *30*). A positive response is determined by the observer noting a consistent head movement by the animal in response to the moving gratings (the stimulus). The MEK inhibitor–treated group not only showed a higher response rate compared to vehicle control (82% versus 44%, $P < 0.05$, n = minimum of 9 mice per group) but also had more robust responses (35%) compared to the vehicle control group (0%, no robust response at all) (Fig. 4H). It is notable that no difference was observed in the retinal histology of wild type, treatment groups, and control groups (fig. S5). These results demonstrate that treatment with topical MEK inhibitor resulted in improved visual function in PAX6 mutant mice and that the beneficial effect was maintained at least 90 days after treatment cessation.

DISCUSSION

In this study, we developed an approach to compensate for the haploinsufficiency of *PAX6*, to reduce the progression of correlated abnormalities, with a focus on ocular manifestations. As noted earlier, PAX6 is one of the master regulators of eye development.

In the mouse eye, development of the cornea begins on embryonic day 8 (E8) and is deemed to be complete by P56 (*31*). The head surface ectoderm interacts with the optic vesicle around E8, to form a lens placode followed by a lens pit around E10 (*31*). The presumptive corneal epithelium separates from the lens vesicle, both of which are derived from head surface ectoderm, around E11 (*31*). Neural crest–derived cells begin to migrate between these structures to form the corneal stroma and endothelium around E12 (*31*). By E15, the basic cellular structures are in place, but attached together.

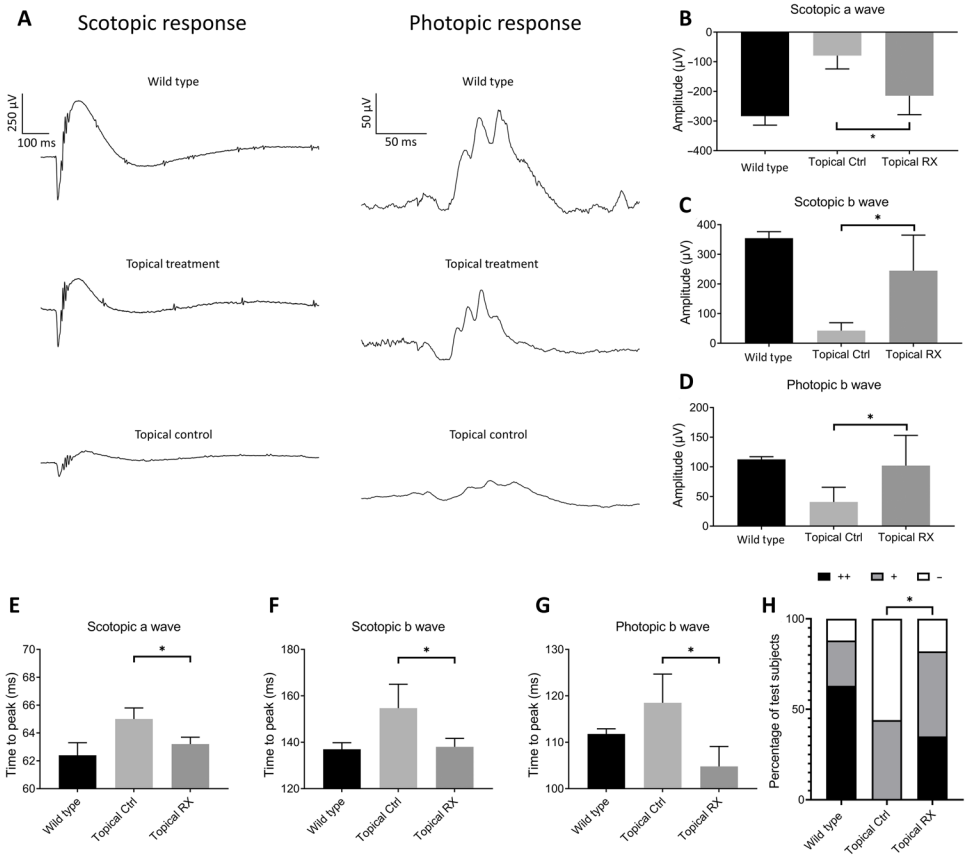

Fig. 4. ERG in response to light stimulation. (**A**) Representative ERG of MEK inhibitor–treated, vehicle control, and wild-type mice in both scotopic and photopic modalities. (**B**) Scotopic a wave amplitude, (**C**) scotopic b wave amplitude, and (**D**) photopic b wave amplitude quantifications ($n = 6$). (**E**) Scotopic a wave, (**F**) scotopic b wave, and (**G**) photopic b wave time-to-peak quantifications ($n = 6$). (**H**) Optomotor testing showing the response to visual stimulus (n = minimum of 9 mice per control/treatment group). Significance determined by t test or Fisher's exact test. *$P < 0.05$. Ctrl, vehicle control. RX, MEK inhibitor treatment. (++) robust optokinetic response, (+) moderate optokinetic response, and (–) no optokinetic response.

They gradually separate to form the lens and lens epithelium, as well as corneal endothelium, stroma, and epithelium by P12 (*31*). The *PAX6* gene plays a major role in nearly all of these developmental events (*31*).

Although the *PAX6* gene has a critical role in the formation and development of several tissues in utero, it continues to be expressed in the adult ocular tissues and is crucial for their function (*9*). Moreover, several abnormalities in congenital aniridia develop and progress postnatally, in particular, the corneal disease, also known as aniridia-related keratopathy (*32*). This provides a potential opportunity to intervene and rescue the ocular tissue from developing further complications. It has been shown that postnatal manipulation of the *PAX6* gene via nonsense suppression can alleviate the ocular manifestations of aniridia (*5*, *17*). In line with these reports, using a different approach to increase *PAX6* protein by inducing the wild-type allele (via MEK inhibition), we showed that early postnatal induction of *PAX6* can alleviate and, in part, prevent the progression of the ocular manifestations of aniridia. We showed that MEK inhibition led to an increase in PAX6 protein in the corneal tissue, which, in turn, led to enhancement of the morphology. Specifically, the treatment led to increased corneal epithelial thickness and differentiation, normalization of the corneal stromal thickness, and less lens-to-cornea adhesions and corneal scarring in mice. The treatment appears to limit the progression of limbal stem cell deficiency, which is the main culprit for secondary conjunctivalization of the cornea, leading to neovascularization and scarring (*27*, *28*).

In this study, rodents were treated up to P30 mainly on the basis of preliminary experiments and the literature (*5*, *17*), indicating the critical period for postnatal eye development to be the first 4 weeks of life. After treatment, the beneficial effects of MEK inhibition appear to be maintained at least up to P90 (60 days after stopping treatment), most notably at the corneal epithelial level as measured by thickness and differentiation. The effects on the stroma appear to be less persistent, and by P60, both oral and topical groups show an increase in thickness. It is worth noting that stromal thickness measurement in this model presents some challenges given the variable thickness of the cornea. We attempted to standardize the measurement by defining a specific location in the central cornea immediately adjacent to the scar (adhesion) area; however, the operator's definition of this location can still vary between investigators (all measurements were done by one person in this study to minimize this variability). Overall, this gradual increase in stromal thickness suggests that a longer duration of therapy may potentially provide additional benefits. Further studies are required to determine the optimal duration of treatment in this particular model. Nonetheless, these results highlight the potential for clinical translation of such interventions in humans where development and progression of the disease are different from murine models.

The treatment also resulted in ERG amelioration, improving the wave patterns and amplitudes. Up to 50 to 70% of human aniridic patients suffer from foveal hypoplasia (an underdeveloped fovea) (*17*). Considering the fact that the fovea is not fully formed until 4 to 5 years of age (*33*, *34*), early postnatal *PAX6* induction could potentially improve foveal development. In the mouse model of aniridia, however, there is no opportunity to assess the foveal hypoplasia since mice do not develop a fovea. Human studies have shown considerable variability in foveal development in patients even with the same *PAX6* mutation, with functional variability within each grade of foveal hypoplasia (*35*). There are also reports of ERG abnormalities in patients with mutations in the *PAX6* gene, suggesting that ERG could be a reasonable functional test to objectively assess the response to potential treatments (*36*). On the other hand, it is well known that opacifications such as marked cataractous lens changes can reduce ERG a and b wave amplitudes (*37*). Considering these, and given that there were no observed changes in the retinal

histological morphology in our study, the improved function of the retina could be interpreted as being mostly the result of less corneal opacity leading to a better light passage and focus on the retina—and perhaps enhanced retinal cellular function—ultimately improving the ocular function as a whole. The beneficial effect of the treatment on visual function was further confirmed with an optomotor response test. The MEK-treated eyes showed higher response rate and more robust visual responses compared to vehicle-treated controls. The above results collectively show that early postnatal induction of the normal (wild type) copy of *PAX6*, through MEK inhibition, could lead to gene dosage compensation with overall improvement in several ocular structural and functional measures.

The stimulation of *PAX6* expression via inducing the wild-type allele hypothetically would have limited efficacy in cases where the mutation in *PAX6* leads to a dominant-negative effect. For instance, some mutations in the proline/serine/threonine-rich region are reported to cause run-on translation into the 3′ untranslated region, resulting in a dominant-negative mutation and a severe aniridia phenotype (*38*, *39*). However, these include only a small portion of the many mutations and deletions, which cause *PAX6*-haploinsufficient aniridia (*39*).

The mechanism of MEK modulation of *PAX6* has been studied before. Studies have shown that *PAX6* has an inverse relationship with proliferation while promoting differentiation in the ocular tissue, particularly corneal epithelium (*40*). The epidermal growth factor receptor kinase–ERK (EGFRK-ERK) pathway has a negative correlation with the expression of *PAX6* (*41*). MEK is upstream from ERK, which leads to phosphorylation and activation of ERK; therefore, MEK inhibition leads to inhibition of ERK pathway, which, in turn, increases *PAX6* expression (*22*). The EGF-induced transcription factor, CTCF, is a negative regulator of the *PAX6* gene in the cornea and retina (*42*). Studies have shown that MEK inhibition prevents up-regulation of CTCF by EGF, subsequently blocking EGF-induced down-regulation of *PAX6*, and allowing for greater *PAX6* expression (*21*). On the other hand, MEK inhibition leads to decreased cell proliferation, which favors *PAX6* expression (*22*). It is interesting to note that *PAX6* can autoregulate its own expression (*43*, *44*). This was mainly evident at the mRNA level after MEK inhibition in nonmutant human corneal epithelial cells, and it was not seen in *PAX6* mutant human corneal stromal cells. This suggests that the response to MEK inhibition can vary depending on the cell type, as well as baseline *PAX6* mRNA expression. We see PAX6 protein expression reach a steady state after MEK inhibition in the nonmutant human corneal epithelial cells. This highlights the complex nature of *PAX6* autoregulation and the need for further studies to determine the effect of MEK inhibition—and inducing the wild-type *PAX6* allele, in general—on these regulatory mechanisms.

Aside from the ocular manifestations, *PAX6* mutations can also lead to dysfunction in other organs including brain, olfactory system, and pancreas (*4*). For instance, it has been shown that *PAX6* is responsible for maintaining pancreatic β cells and keeping their balance with other islet cell types, mainly via activating β cell genes and maintaining mature β cell function and identity, while repressing alternative islet cell genes such as ghrelin, glucagon, and somatostatin (*7*). Thus, reduced expression of *PAX6* may contribute to β cell failure and α cell dysfunction in diabetes (*7*). Likewise, *PAX6* has crucial roles in brain development and function (*8*), via balancing proliferation and differentiation of neural progenitor cells (*45*). After birth, biological and functional development of the brain continues until early adulthood (*45*). Reductions in *PAX6* expression has been shown to be associated with several neuronal developmental conditions, such as autism (*8*). Oral treatment with MEK inhibitors could be considered in these systems as a potential therapy for modulating islet cell function, as well as for promoting neural progenitor cells' favorable proliferation and differentiation.

Although there have been reports of ocular toxicity with systemic MEK inhibitors, most notably self-limited serous retinal detachment and occasional retinal vein occlusion, these side effects were shown to be dose dependent, happening typically above 20 to 30 mg/day (*46*, *47*). The effective dosage in this study is much less than the toxic dosage (equivalent dosage for human is 0.125 mg/kg per day orally and 1 μg/day topically) (*48*). Furthermore, we did not observe histological changes in the retina of the treated mice. On the other hand, low-dose MEK inhibition has been shown to have beneficial effects, such as anti-aging and improving late-life health (*49*). Low-dose inhibition of MEK has also been shown to moderate the developmental effects of $BRAF^{CFC}$ mutations, specifically ameliorating the cardiofaciocutaneous phenotype (*50*). The MEK inhibitor PD0325901 has also been tested during development in pregnant mice and was shown to rescue the myopathic features of neurofibromatosis type 1 in the pups (*51*). These studies provide evidence in support of the safety and potential efficacy of low-dose MEK inhibition. Nonetheless, the primary aim of the present study was to show the efficacy of pharmacologic gene dosage enhancement in this condition, and MEK inhibitors were used as a representative agent and there are likely other repurposed drug candidates that could be used in this setting.

There are a number of limitations to the findings of this study. First, because the study was conducted in mice, it may not represent what takes place in patients where eye development and disease follow a very different time course. Likewise, this study could not completely assess all the possible toxic effects of topical MEK inhibitor, and for instance, the effects on intraocular pressure or cataract formation with more long-term use were not assessed. Therefore, more preclinical safety studies with a range of doses and durations are clearly warranted before clinical translation.

In conclusion, early postnatal induction of the healthy copy of *PAX6* can alleviate several manifestations of *PAX6*-deficient aniridia. This approach can be potentially useful for treating and/or preventing aniridia-related abnormalities, particularly the progressive corneal disease, in children born with this devastating condition. The topical treatment not only was more effective but also limits the potential systemic side effects of the treatment. Considering that at least 500 different mutations are known to cause *PAX6*-deficient aniridia in humans (*5*, *52*), the approach to stimulate the normal copy has the advantage of not being limited by the type of mutation (except as noted above). Furthermore, it suggests that using a drug repurposing strategy of inducing the wild-type allele could be implemented clinically for gene dosage compensation in other haploinsufficiencies.

MATERIALS AND METHODS

Study design

In this study, we hypothesized that induction of the wild-type allele in *PAX6* haploinsufficiency could lead to gene dosage compensation and mitigation of the ocular abnormalities. Using a targeted chemical screen based on the related pathways, we identified MEK

inhibitors as inducers of *PAX6* and tested our hypothesis in both healthy and mutant corneal cells in vitro, and in a mouse model of the disease ($Pax6^{Sey\text{-}Neu/+}$) in vivo.

Sample size was determined using the "resource equation" method, which is the recommended choice for studies involving complex biological experiments that include several treatment groups, when multiple end points are measured (*53*, *54*). Briefly, according to this method, a value "*E*" is measured, which is the degree of freedom of analysis of variance (ANOVA). The experiment should be of an appropriate size *E* (between 10 and 20). If *E* is more than 20, adding more animals will not increase the chance of getting significant results (*53*, *54*)

$$E = \text{total number of animals} - \text{total number of groups}$$

On the basis of this equation, a minimum of five mice per group was used to ensure detection of a significant difference between groups. Animals were tagged, coded, and randomly put into groups. All the treatment and statistical analysis were done in a blinded fashion, and the results were decoded afterward.

In vitro treatments

HCLE cell line (telomerase-immortalized human corneal-limbal epithelial cell) and freshly isolated primary human corneal epithelial cells were cultured in keratinocyte serum-free medium (KSFM; Invitrogen) as previously described (*55*, *56*). To isolate human corneal epithelial cell, cadaver corneas (provided by Eversight) were treated with dispase (2 mg/ml; Thermo Fisher Scientific) at 37°C for 2 hours to separate the epithelial sheets, which were then separated and digested in 0.25% trypsin-EDTA for 10 min, and filtered through a 70-μm nylon strainer to obtain a single-cell suspension. Cells were washed and resuspended in KSFM and plated in collagen-coated tissue culture plates. Cells from passage zero were used for all of our experiments.

Corneal mesenchymal stromal cells were isolated from *PAX6*-deficient mice ($Pax6^{Sey\text{-}Neu/+}$) as previously described (*57*). Briefly, mice corneas were enucleated and washed five times with phosphate-buffered saline (PBS) containing 2× antibiotic-antimycotic and 2× penicillin-streptomycin (Thermo Fisher Scientific). The limbus was cut into three segments that were placed in 2.4 IU of dispase (Thermo Fisher Scientific) for 1 hour at 37°C. Intact epithelial sheets were removed from stroma, and the stroma was used directly for explant culture in 1% gelatin (Sigma-Aldrich)–coated wells of a six-well tissue culture plate in alpha minimum essential medium supplemented with 10% fetal bovine serum, 1× L-glutamine, and 1× Nonessential Amino Acids (NEAA) (all from Corning). Culture media were changed every other day, and cells were subcultured by brief digestion with reagent (TrypLE Express; Thermo Fisher Scientific) when 80% confluent.

Treatments were done in six-well plates. Upon 70% confluency, the cells were treated with either 1 μM PD0325901 or 1:50,000 DMSO (vehicle control), 1 μM cobimetinib or 1:47,000 DMSO (vehicle control), and 1 μM refametinib or 1:35,000 ethanol (vehicle control).

Western blot

Protein expression was compared using Western blots as previously described (*56*). Briefly, cells were lysed (CelLytic, Sigma-Aldrich), and after measuring protein concentration [Bicinchoninic acid assay (BCA); Thermo Fisher Scientific], equal amounts of each sample were mixed with Laemmli sample buffer (Bio-Rad), denatured by heating at 70°C for 10 min, and subjected to electrophoresis on NuPAGE 4 to 12% bis-tris gel (Invitrogen). After gel electrophoresis, the proteins were transferred to polyvinylidine fluoride membranes using iBlot gel transfer (Invitrogen). The membranes were then incubated in 5% bovine serum albumin in tris-buffered saline with 0.01% Tween 20 (TBST) for 1 hour, followed by incubation with primary antibody while shaking in 4°C overnight. After washes with TBST and incubation with respective horseradish peroxidase–conjugated secondary antibodies for 1 hour in room temperature, protein bands were visualized using the SuperSignal West Femto maximum sensitivity substrate (Thermo Fisher Scientific) with an ImageQuant LAS 4000 biomolecular imager (GE Healthcare Life Sciences).

The following antibodies were used: PAX6, ab5790 from Abcam; mitogen-activated protein kinase (MAPK) family including p44/42 and p38, #9926 from Cell Signaling Technology; phospho-MAPK family including Pp44/42 and Pp38, #9910 from Cell Signaling Technology; and glyceraldehyde-3-phosphate dehydrogenase, sc-66163 from Santa Cruz Biotechnology.

Polymerase chain reaction

RNA expression was compared using polymerase chain reaction (PCR) as previously described (*55*). Briefly, total RNA was extracted from treated cells (TRIzol; Life Technologies) according to the manufacturer's protocol. After spectrophotometric assessment for quality and concentration (Nanodrop ND-1000; Thermo Fisher Scientific), complementary DNAs (cDNAs) were generated via the High Capacity cDNA Reverse Transcription Kit (Applied Biosystems) using the manufacturer's protocol. For each reaction, 2 μg of total RNA was used. The quantitative PCR reactions were carried out in triplicate with FastStart Universal SYBER GREEN Master (Roche) in a total volume of 20 μl, using thermal cycling conditions of 10 min at 90°C and 10 s at 95°C, followed by 40 cycles of 95°C for 15 s and 60°C for 1 min. Three different *PAX6* primer pairs were used: 5′-CCG-TGT-GCC-TCA-ACC-GTA-3′ and 5′-CAC-GGT-TTA-CTG-GGT-CTG-G-3′, 5′-ATG-GTT-TTC-TAA-TCG-AAG-GG-3′ and 5′-CGG-TGT-GGT-GGG-TTG-TGG-AAT-3′, and 5′-TCT-TTG-CTT-GGG-AAA-TCC-G-3′ and 5′-CTG-CCC-GTT-CAA-CAT-CCT-TAG-3′. The results are presented as means of these three.

In vivo treatments

All the procedures were conducted in compliance with the recommendations of the Association for Research in Vision and Ophthalmology. The protocol was approved by the Committee on the Ethics of Animal Experiments of the University of Illinois at Chicago.

A mouse model of *PAX6*-deficient aniridia ($Pax6^{Sey\text{-}Neu/+}$) on BalB/c background, provided by J. D. Lauderdale, was used in this study. The mice were genotyped to assure that they have the mutation for the treatment and vehicle control groups, and the wild-type littermates were used as normal reference. Murine oral treatment dosage was 1.5 mg/kg per day, which was based on the literature to reach the optimal therapeutic dosage in the bloodstream (*47*, *58*). The optimized formulation was 5 mM PD0325901 and 10% DMSO in PBS. To optimize the topical preparation, several dosages and formulations were tested, and the highest effective dose that had the optimum viscosity (to maximize the drug interaction time with the cornea, using hydroxypropyl methylcellulose) and did not cause irritation was chosen (1 mM PD0325901, 2% DMSO, and 2% hydroxypropyl methylcellulose, in PBS, once a day for 5 days, then a 2-day break, and repeat, for a total of 4 weeks). The treatment method

of 5 days on and 2 days off was based on previous clinical studies on PD0325901, aimed at preventing saturation of the pathway and minimizing the potential side effects (*47*). Oral or topical treatment or vehicle control was administered to the mice starting from P5, until P30. The oral treatment was done once a day, with 10 μl of solution orally, and the topical treatment was applied once a day as 25 μl of solution per eye, without anesthesia. A minimum of six mice were used per each group.

OCT and slit lamp measurement of corneal opacity

The mice were anesthetized by intraperitoneal injection of ketamine (100 mg/kg) and xylazine (5 mg/kg) mixture and underwent OCT imaging (Phoenix MICRON IV) and slit lamp imaging (Nikon). Corneal epithelial and stromal thicknesses were measured at the central cornea and outside the scar area via OCT imaging. The area of scarring was measured manually based on the corneal opacification in the scar area on the slit lamp images using ImageJ [National Institutes of Health (NIH)]. The ratio of the scar area to total corneal area was reported as a percentage.

Immunostaining

Immunostaining of mouse eye cryo-sections at P30 and corneal whole mount at P90 were performed as previously described (*59*, *60*). Briefly, dissected corneas were fixed with 4% paraformaldehyde at 4°C overnight. After washing with PBS, they were incubated with proteinase-K (20 μg/ml; Sigma-Aldrich) for 5 min at room temperature followed by 100% methanol for another 30 min. The cryosections were fixed for 10 min in chilled paraformaldehyde and blocked at room temperature with 10% donkey serum for 1 hour.

The samples were incubated overnight at 4°C with primary antibody. For negative controls, the sections were incubated without the primary antibody. After washing three times with TBST, the secondary antibody was applied for 1 hour at room temperature followed by counterstaining with 4′,6-diamidino-2-phenylindole (DAPI).

Antibodies included primary antibodies against PAX6 (ab195045, Abcam), CK12 (sc-25722, Santa Cruz Biotechnology), Ki67 (#4203-1, Epitomics), and fluorescein-conjugated secondary antibodies (Jackson ImmunoResearch). Imaging was performed with the same light intensity and exposure for all the samples, using a confocal microscope (LSM 710, Carl Zeiss). The results were analyzed with ImageJ (NIH) and were standardized on the basis of the wild-type intensity.

Electroretinography

ERG to record the responses of the retina to light flashes was performed as previously described (*61*). Dark-adapted responses were recorded at P90 after 2-hour dark adaptation by averaging four responses at a stimulus intensity of 3 cd·s/m^2. Light-adapted cone responses were carried out in 5 cd/m^2 background light to saturate rods.

Optomotor test

Mouse optomotor response was tested using the PhenoSys qOMR system (PhenoSys GmbH). In brief, each mouse was placed on an elevated central platform surrounded by four monitors to evoke an optokinetic response (*62*–*65*). After 5 to 10 min of adaptation with a gray screen, vertical stripes moving horizontally at spatial frequencies of 0.09 and 0.11 cycles per degree were presented to the mouse for 2 min (*66*, *67*). The spatial frequencies of 0.09 and 0.11 cycles per degree were used here because the BalB/c wild-type mice exhibited consistent and identifiable responses to the visual stimulus (*62*). The gratings were alternating clockwise and counterclockwise for 10 s in each direction during the 2 min (a total of 12 gratings). The mouse's responses were recorded as follows: (i) ++, robust and consistent reflective head movement observed in response to the gratings, ≥4 times; (ii) +, moderate but less robust reflective head movement in response to the gratings, 1 to 3 times; and (iii) −, no head movement in response to alternating gratings during the 2-min test. Animals' responses were videotaped with infrared camera and re-examined by a second observer for confirmation when needed. Experimenters were blinded to the mouse genotypes and experimental groups. Results were analyzed and plotted by a third experimenter.

Statistical analysis

All the experiments were replicated three times. The in vivo experiments were done in groups of at least five mice, and one eye per mouse was used for analysis to minimize bias. We randomly selected the right eye for all subjects to minimize variations. All the analyses were performed blinded, using GraphPad Prism 7.0, and an unpaired two-tailed Student's *t* test or one-way ANOVA followed by Tukey's multiple comparison test were used when appropriate. $P < 0.05$ was considered significant. Results are reported as mean ± SD.

SUPPLEMENTARY MATERIALS

stm.sciencemag.org/cgi/content/full/12/573/eaaz4894/DC1

Fig. S1. Comparing the results of P0325901 treatment on P30, from different start points with OCT.

Fig. S2. Wild-type mice were treated postnatally (P5 to P30) with oral or topical formulations of PD0325901 to assess any possible adverse effect of MEK inhibition.

Fig. S3. Maintenance of MEK inhibitor treatment effects on P60 (30 days after stopping the treatment) in *Pax6*$^{Sey\text{-}Neu/+}$ mice.

Fig. S4. The eyes were enucleated on P90, and axial lengths were measured.

Fig. S5. Retinal histology of P30 mice.

Data file S1. Raw data (provided as separate Excel file).

View/request a protocol for this paper from *Bio-protocol*.

REFERENCES AND NOTES

1. T. I. Simpson, D. J. Price, Pax6; a pleiotropic player in development. *Bioessays* **24**, 1041–1051 (2002).
2. C. C. Ton, H. Hirvonen, H. Miwa, M. M. Weil, P. Monaghan, T. Jordan, V. van Heyningen, N. D. Hastie, H. Meijers-Heijboer, M. Drechsler, B. Royer-Pokora, F. Collines, A. Swaroop, L. C. Strong, G. F. Saunders, Positional cloning and characterization of a paired box- and homeobox-containing gene from the aniridia region. *Cell* **67**, 1059–1074 (1991).
3. J. Yeung, T. J. Ha, D. J. Swanson, D. Goldowitz, A novel and multivalent role of Pax6 in cerebellar development. *J. Neurosci.* **36**, 9057–9069 (2016).
4. S. M. Sisodiya, S. L. Free, K. A. Williamson, T. N. Mitchell, C. Willis, J. M. Stevens, B. E. Kendall, S. D. Shorvon, I. M. Hanson, A. T. Moore, V. van Heyningen, PAX6 haploinsufficiency causes cerebral malformation and olfactory dysfunction in humans. *Nat. Genet.* **28**, 214–216 (2001).
5. C. Y. Gregory-Evans, X. Wang, K. M. Wasan, J. Zhao, A. L. Metcalfe, K. Gregory-Evans, Postnatal manipulation of Pax6 dosage reverses congenital tissue malformation defects. *J. Clin. Invest.* **124**, 111–116 (2014).
6. M. Hingorani, I. Hanson, V. van Heyningen, Aniridia. *Eur. J. Hum. Genet.* **20**, 1011–1017 (2012).
7. A. Swisa, D. Avrahami, N. Eden, J. Zhang, E. Feleke, T. Dahan, Y. Cohen-Tayar, M. Stolovich-Rain, K. H. Kaestner, B. Glaser, R. Ashery-Padan, Y. Dor, PAX6 maintains β cell identity by repressing genes of alternative islet cell types. *J. Clin. Invest.* **127**, 230–243 (2017).
8. T. Kikkawa, C. R. Casingal, S. H. Chun, H. Shinohara, K. Hiraoka, N. Osumi, The role of *Pax6* in brain development and its impact on pathogenesis of autism spectrum disorder. *Brain Res.* **1705**, 95–103 (2019).
9. E. I. Traboulsi, in *Ocular Disease* (Elsevier, 2010), pp. 472–477.
10. S. Nishina, S. Kohsaka, Y. Yamaguchi, H. Handa, A. Kawakami, H. Fujisawa, N. Azuma, PAX6 expression in the developing human eye. *Br. J. Ophthalmol.* **83**, 723–727 (1999).

11. J. Davis, M. K. Duncan, W. G. Robison Jr., J. Piatigorsky, Requirement for Pax6 in corneal morphogenesis: A role in adhesion. *J. Cell Sci.* **116**, 2157–2167 (2003).
12. N. J. Dorà, M. Manuel, D.-J. Kleinjan, D. J. Price, J. M. Collinson, R. E. Hill, J. D. West, A conditional Pax6 depletion study with no morphological effect on the adult mouse corneal epithelium. *BMC. Res. Notes* **11**, 705 (2018).
13. N. Osumi, H. Shinohara, K. Numayama-Tsuruta, M. Maekawa, Concise review: Pax6 transcription factor contributes to both embryonic and adult neurogenesis as a multifunctional regulator. *Stem Cells* **26**, 1663–1672 (2008).
14. V. van Heyningen, K. A. Williamson, PAX6 in sensory development. *Hum. Mol. Genet.* **11**, 1161–1167 (2002).
15. N. Matharu, S. Rattanasopha, S. Tamura, L. Maliskova, Y. Wang, A. Bernard, A. Hardin, W. L. Eckalbar, C. Vaisse, N. Ahituv, CRISPR-mediated activation of a promoter or enhancer rescues obesity caused by haploinsufficiency. *Science* **363**, eaau0629 (2019).
16. A. Yasue, H. Kono, M. Habuta, T. Bando, K. Sato, J. Inoue, S. Oyadomari, S. Noji, E. Tanaka, H. Ohuchi, Relationship between somatic mosaicism of *Pax6* mutation and variable developmental eye abnormalities—An analysis of CRISPR genome-edited mouse embryos. *Sci. Rep.* **7**, 53 (2017).
17. X. Wang, K. Gregory-Evans, K. M. Wasan, O. Sivak, X. Shan, C. Y. Gregory-Evans, Efficacy of postnatal in vivo nonsense suppression therapy in a *Pax6* mouse model of aniridia. *Mol. Ther. Nucleic Acids* **7**, 417–428 (2017).
18. A. E. Arrant, V. C. Onyilo, D. E. Unger, E. D. Roberson, Progranulin gene therapy improves lysosomal dysfunction and microglial pathology associated with frontotemporal dementia and neuronal ceroid lipofuscinosis. *J. Neurosci.* **38**, 2341–2358 (2018).
19. S. Tu, M. W. Akhtar, R. M. Escorihuela, A. Amador-Arjona, V. Swarup, J. Parker, J. D. Zaremba, T. Holland, N. Bansal, D. R. Holohan, K. Lopez, S. D. Ryan, S. F. Chan, L. Yan, X. Zhang, X. Huang, A. Sultan, S. R. McKercher, R. Ambasudhan, H. Xu, Y. Wang, D. H. Geschwind, A. J. Roberts, A. V. Terskikh, R. A. Rissman, E. Masliah, S. A. Lipton, N. Nakanishi, NitroSynapsin therapy for a mouse MEF2C haploinsufficiency model of human autism. *Nat. Commun.* **8**, 1488 (2017).
20. T. Ramaesh, J. M. Collinson, K. Ramaesh, M. H. Kaufman, J. D. West, B. Dhillon, Corneal abnormalities in $Pax6^{+/-}$ small eye mice mimic human aniridia-related keratopathy. *Invest. Ophthalmol. Vis. Sci.* **44**, 1871–1878 (2003).
21. T. Li, L. Lu, Epidermal growth factor-induced proliferation requires down-regulation of Pax6 in corneal epithelial cells. *J. Biol. Chem.* **280**, 12988–12995 (2005).
22. P. de la Puente, B. Muz, A. Jin, F. Azab, M. Luderer, N. N. Salama, A. K. Azab, MEK inhibitor, TAK-733 reduces proliferation, affects cell cycle and apoptosis, and synergizes with other targeted therapies in multiple myeloma. *Blood Cancer J.* **6**, e399 (2016).
23. Y. Isshiki, Y. Kohchi, H. Iikura, Y. Matsubara, K. Asoh, T. Murata, M. Kohchi, E. Mizuguchi, S. Tsujii, K. Hattori, T. Miura, Y. Yoshimura, S. Aida, M. Miwa, R. Saitoh, N. Murao, H. Okabe, C. Belunis, C. Janson, C. Lukacs, V. Schück, N. Shimma, Design and synthesis of novel allosteric MEK inhibitor CH4987655 as an orally available anticancer agent. *Bioorg. Med. Chem. Lett.* **21**, 1795–1801 (2011).
24. Y. Cheng, H. Tian, Current development status of MEK inhibitors. *Molecules* **22**, 1551 (2017).
25. K. Capriotti, J. A. Capriotti, Dimethyl sulfoxide: History, chemistry, and clinical utility in dermatology. *J. Clin. Aesthet. Dermatol.* **5**, 24–26 (2012).
26. W. Li, Y.-T. Chen, Y. Hayashida, G. Blanco, A. Kheirkah, H. He, S.-Y. Chen, C.-Y. Liu, S. Tseng, Down-regulation of Pax6 is associated with abnormal differentiation of corneal epithelial cells in severe ocular surface diseases. *J. Pathol.* **214**, 114–122 (2008).
27. G. Li, F. Xu, J. Zhu, M. Krawczyk, Y. Zhang, J. Yuan, S. Patel, Y. Wang, Y. Lin, M. Zhang, G. Cao, E. Yeh, D. Lin, Q. Su, W.-w. Li, G. L. Sen, N. Afshari, S. Chen, R. L. Maas, X.-D. Fu, K. Zhang, Y. Liu, H. Ouyang, Transcription factor PAX6 (paired box 6) controls limbal stem cell lineage in development and disease. *J. Biol. Chem.* **290**, 20448–20454 (2015).
28. H. M. Skeens, B. P. Brooks, E. J. Holland, Congenital aniridia variant: Minimally abnormal irides with severe limbal stem cell deficiency. *Ophthalmology* **118**, 1260–1264 (2011).
29. J. Abdeljalil, M. Hamid, O. Abdel-Mouttalib, R. Stéphane, R. Raymond, A. Johan, S. José, C. Pierre, P. Serge, The optomotor response: A robust first-line visual screening method for mice. *Vision Res.* **45**, 1439–1446 (2005).
30. C. Shi, X. Yuan, K. Chang, K.-S. Cho, X. S. Xie, D. F. Chen, G. Luo, Optimization of optomotor response-based visual function assessment in mice. *Sci. Rep.* **8**, 9708 (2018).
31. S. K. Swamynathan, Ocular surface development and gene expression. *J. Ophthalmol.* **2013**, 103947 (2013).
32. L. N. Roux, I. Petit, R. Domart, J.-P. Concordet, J. Qu, H. Zhou, A. Joliot, O. Ferrigno, D. Aberdam, Modeling of aniridia-related keratopathy by CRISPR/Cas9 genome editing of human limbal epithelial cells and rescue by recombinant PAX6 protein. *Stem Cells* **36**, 1421–1429 (2018).
33. C. Y. Gregory-Evans, K. Gregory-Evans, Foveal hypoplasia: The case for arrested development. *Expert Rev. Ophthalmol.* **6**, 565–574 (2011).
34. A. Hendrickson, D. Possin, L. Vajzovic, C. A. Toth, Histologic development of the human fovea from midgestation to maturity. *Am. J. Ophthalmol.* **154**, 767–778.e2 (2012).
35. H. R. Pedersen, M. Neitz, S. J. Gilson, E. C. Landsend, Ø. A. Utheim, T. P. Utheim, R. C. Baraas, The cone photoreceptor mosaic in aniridia: Within-family phenotype–genotype discordance. *Ophthalmol. Retina* **3**, 523–534 (2019).
36. M. P. Hood, N. C. Kerr, N. Smaoui, A. Iannaccone, Abnormal cone ERGs in a family with congenital nystagmus and photophobia harboring a p.X423Lfs mutation in the PAX6 gene. *Doc. Ophthalmol.* **130**, 157–164 (2015).
37. G. A. Fishman, Basic principles of clinical electroretinography. *Retina* **5**, 123–126 (1985).
38. S. Aggarwal, W. Jinda, C. Limwongse, L.-o. Atchaneeyasakul, S. R. Phadke, Run-on mutation in the PAX6 gene and chorioretinal degeneration in autosomal dominant aniridia. *Mol. Vis.* **17**, 1305–1309 (2011).
39. T. Yokoi, S. Nishina, M. Fukami, T. Ogata, K. Hosono, Y. Hotta, N. Azuma, Genotype–phenotype correlation of *PAX6* gene mutations in aniridia. *Hum. Genome Var.* **3**, 15052 (2016).
40. J. Ouyang, Y.-C. Shen, L.-K. Yeh, W. Li, B. M. Coyle, C.-Y. Liu, M. E. Fini, Pax6 overexpression suppresses cell proliferation and retards the cell cycle in corneal epithelial cells. *Invest. Ophthalmol. Vis. Sci.* **47**, 2397–2407 (2006).
41. F. Shi, Y. Fan, L. Zhang, L. Meng, H. Zhi, H. Hu, A. Lin, The expression of Pax6 variants is subject to posttranscriptional regulation in the developing mouse eyelid. *PLOS ONE* **8**, e53919 (2013).
42. J. Gao, J. Wang, Y. Wang, W. Dai, L. Lu, Regulation of *Pax6* by CTCF during induction of mouse ES cell differentiation. *PLOS ONE* **6**, e20954 (2011).
43. S.-i. Aota, N. Nakajima, R. Sakamoto, S. Watanabe, N. Ibaraki, K. Okazaki, *Pax6* autoregulation mediated by direct interaction of *Pax6* protein with the head surface ectoderm-specific enhancer of the mouse Pax6 gene. *Dev. Biol.* **257**, 1–13 (2003).
44. M. Manuel, P. A. Georgala, C. B. Carr, S. Chanas, D. A. Kleinjan, B. Martynoga, J. O. Mason, M. Molinek, J. Pinson, T. Pratt, J. C. Quinn, T. I. Simpson, D. A. Tyas, V. van Heyningen, J. D. West, D. J. Price, Controlled overexpression of Pax6 in vivo negatively autoregulates the *Pax6* locus, causing cell-autonomous defects of late cortical progenitor proliferation with little effect on cortical arealization. *Development* **134**, 545–555 (2007).
45. N. Warren, D. Caric, T. Pratt, J. A. Clausen, P. Asavaritikrai, J. O. Mason, R. E. Hill, D. J. Price, The transcription factor, *Pax6*, is required for cell proliferation and differentiation in the developing cerebral cortex. *Cereb. Cortex* **9**, 627–635 (1999).
46. J. H. Francis, L. A. Habib, D. H. Abramson, L. A. Yannuzzi, M. Heinemann, M. M. Gounder, R. N. Grisham, M. A. Postow, A. N. Shoushtari, P. Chi, N. H. Segal, R. Yaeger, A. L. Ho, P. B. Chapman, F. Catalanotti, Clinical and morphologic characteristics of MEK inhibitor–associated retinopathy: Differences from central serous chorioretinopathy. *Ophthalmology* **124**, 1788–1798 (2017).
47. P. M. LoRusso, S. S. Krishnamurthi, J. J. Rinehart, L. M. Nabell, L. Malburg, P. B. Chapman, S. E. DePrimo, S. Bentivegna, K. D. Wilner, W. Tan, A. D. Ricart, Phase I pharmacokinetic and pharmacodynamic study of the oral MAPK/ERK kinase inhibitor PD-0325901 in patients with advanced cancers. *Clin. Cancer Res.* **16**, 1924–1937 (2010).
48. A. B. Nair, S. Jacob, A simple practice guide for dose conversion between animals and human. *J. Basic Clin. Pharm.* **7**, 27–31 (2016).
49. J. I. Castillo-Quan, L. S. Tain, K. J. Kinghorn, L. Li, S. Grönke, Y. Hinze, T. K. Blackwell, I. Bjedov, L. Partridge, A triple drug combination targeting components of the nutrient-sensing network maximizes longevity. *Proc. Natl. Acad. Sci. U.S.A.* **116**, 20817–20819 (2019).
50. C. Anastasaki, K. A. Rauen, E. E. Patton, Continual low-level MEK inhibition ameliorates cardio-facio-cutaneous phenotypes in zebrafish. *Dis. Model. Mech.* **5**, 546–552 (2012).
51. M. A. Summers, E. R. Vasiljevski, K. Mikulec, L. Peacock, D. G. Little, A. Schindeler, Developmental dosing with a MEK inhibitor (PD0325901) rescues myopathic features of the muscle-specific but not limb-specific Nf1 knockout mouse. *Mol. Genet. Metab.* **123**, 518–525 (2018).
52. D. Lima Cunha, G. Arno, M. Corton, M. Moosajee, The spectrum of *PAX6* mutations and genotype-phenotype correlations in the eye. *Genes* **10**, 1050 (2019).
53. M. F. Festing, Design and statistical methods in studies using animal models of development. *Ilar J.* **47**, 5–14 (2006).
54. J. Charan, N. Kantharia, How to calculate sample size in animal studies? *J. Pharmacol. Pharmacother.* **4**, 303–306 (2013).
55. S. Gidfar, F. Y. Milani, B. Y. Milani, X. Shen, M. Eslani, I. Putra, M. J. Huvard, H. Sagha, A. R. Djalilian, Rapamycin prolongs the survival of corneal epithelial cells in culture. *Sci. Rep.* **7**, 40308 (2017).
56. I. Putra, B. Rabiee, K. N. Anwar, S. Gidfar, X. Shen, M. Babalooee, M. Ghassemi, N. Afsharkhamseh, S. Bakhsh, D. Missiakas, A. Nezamabadi, B. Milani, M. Eslani, A. R. Djalilian, *Staphylococcus aureus* alpha-hemolysin impairs corneal epithelial wound healing and promotes intracellular bacterial invasion. *Exp. Eye Res.* **181**, 263–270 (2019).
57. M. Eslani, I. Putra, X. Shen, J. Hamouie, N. Afsharkhamseh, S. Besharat, M. I. Rosenblatt, R. Dana, P. Hematti, A. R. Djalilian, Corneal mesenchymal stromal cells are directly antiangiogenic via PEDF and sFLT-1. *Invest. Ophthalmol. Vis. Sci.* **58**, 5507–5517 (2017).
58. J. A. Paulo, F. E. McAllister, R. A. Everley, S. A. Beausoleil, A. S. Banks, S. P. Gygi, Effects of MEK inhibitors GSK1120212 and PD0325901 in vivo using 10-plex quantitative proteomics and phosphoproteomics. *Proteomics* **15**, 462–473 (2015).
59. H. Amirjamshidi, B. Milani, H. Sagha, A. Movahedan, M. Shafiq, R. M. Lavker, B. Yue, A. Djalilian, Limbal fibroblast conditioned media: A non-invasive treatment for limbal stem cell deficiency. *Mol. Vis.* **17**, 658–666 (2011).
60. M. Eslani, I. Putra, X. Shen, J. Hamouie, A. Tadepalli, K. N. Anwar, J. A. Kink, S. Ghassemi, G. Agnihotri, S. Reshetylo, A. Mashaghi, R. Dana, P. Hematti, A. R. Djalilian, Cornea-derived

mesenchymal stromal cells therapeutically modulate macrophage immunophenotype and angiogenic function. *Stem Cells* **36**, 775–784 (2018).
61. D. J. Ramsey, H. Ripps, H. Qian, An electrophysiological study of retinal function in the diabetic female rat. *Invest. Ophthalmol. Vis. Sci.* **47**, 5116–5124 (2006).
62. K. V. Rangarajan, C. Lawhn-Heath, L. Feng, T. S. Kim, J. Cang, X. Liu, Detection of visual deficits in aging DBA/2J mice by two behavioral assays. *Curr. Eye Res.* **36**, 481–491 (2011).
63. L. Wang, K. V. Rangarajan, C. A. Lawhn-Heath, R. Sarnaik, B.-S. Wang, X. Liu, J. Cang, Direction-specific disruption of subcortical visual behavior and receptive fields in mice lacking the β2 subunit of nicotinic acetylcholine receptor. *J. Neurosci.* **29**, 12909–12918 (2009).
64. H. Chen, Y. Zhao, M. Liu, L. Feng, Z. Puyang, J. Yi, P. Liang, H. F. Zhang, J. Cang, J. B. Troy, X. Liu, Progressive degeneration of retinal and superior collicular functions in mice with sustained ocular hypertension. *Invest. Ophthalmol. Vis. Sci.* **56**, 1971–1984 (2015).
65. L. Feng, H. Chen, J. Yi, J. B. Troy, H. F. Zhang, X. Liu, Long-term protection of retinal ganglion cells and visual function by brain-derived neurotrophic factor in mice with ocular hypertension. *Invest. Ophthalmol. Vis. Sci.* **57**, 3793–3802 (2016).
66. N. Yeritsyan, K. Lehmann, O. Puk, J. Graw, S. Löwel, Visual capabilities and cortical maps in BALB/c mice. *Eur. J. Neurosci.* **36**, 2801–2811 (2012).
67. B. R. Thomson, M. Grannonico, F. Liu, M. Liu, P. Mendapara, Y. Xu, X. Liu, S. E. Quaggin, Angiopoietin-1 knockout mice as a genetic model of open-angle glaucoma. *Transl. Vis. Sci. Technol.* **9**, 16 (2020).

Acknowledgments: We thank R. Zelkha for help in microscopic imaging. **Funding:** This work was supported by R01-EY024349 (A.R.D.), Core grant EY01792 (M.I.R.), and R01EY026286 and R01EY029121 (X.L.) all from NEI/NIH; Vision For Tomorrow (A.R.D.) and Unrestricted Grant to the Department (M.I.R.) and Physician-Scientist Award (A.R.D.) both from Research to Prevent Blindness; and Eversight (A.R.D.). **Author contributions:** B.R. conducted cell culture, in vitro treatment, Western blot, animal experiments, immunostaining, data gathering, and imaging. K.N.A. helped with group coding and blinding B.R. to the groups and conducted PCR. X.S. helped with animal maintenance and Western blot. M.L. conducted the optomotor tests. I.P. and N.A. helped with animal maintenance and imaging. B.R. analyzed the data and wrote the manuscript. R.J. helped with the in vitro experiments and literature review. M.G., M.I.R., X.L., and G.A.F. contributed scientific discussion and revised the manuscript. A.R.D. designed and supervised the studies and finalized the manuscript. **Competing interests:** A patent application partially covering this work has been filed by the University of Illinois (US20/30150, MEK Inhibitors for Corneal Scarring and Neovascularization). A.R.D. is a consultant for Novartis, Combangio, and Dompé, none of which are related to the present work. M.I.R. is a consultant for Laurel Therapeutics, Silk Tears, Roche, AbbVie, Sarentis Therapeutics, and PanOptica, none of which are related to the present work. All other authors declare that they have no competing interests. **Data and materials availability:** All data associated with this study are present in the paper or the Supplementary Materials.

Submitted 12 September 2019
Resubmitted 16 April 2020
Accepted 4 September 2020
Published 9 December 2020
10.1126/scitranslmed.aaz4894

Citation: B. Rabiee, K. N. Anwar, X. Shen, I. Putra, M. Liu, R. Jung, N. Afsharkhamseh, M. I. Rosenblatt, G. A. Fishman, X. Liu, M. Ghassemi, A. R. Djalilian, Gene dosage manipulation alleviates manifestations of hereditary *PAX6* haploinsufficiency in mice. *Sci. Transl. Med.* **12**, eaaz4894 (2020).

Science Translational Medicine

Gene dosage manipulation alleviates manifestations of hereditary *PAX6* haploinsufficiency in mice

Behnam Rabiee, Khandaker N. Anwar, Xiang Shen, Ilham Putra, Mingna Liu, Rebecca Jung, Neda Afsharkhamseh, Mark I. Rosenblatt, Gerald A. Fishman, Xiaorong Liu, Mahmood Ghassemi and Ali R. Djalilian

Sci Transl Med **12**, eaaz4894.
DOI: 10.1126/scitranslmed.aaz4894

Eye-opening treatment for haploinsufficiency

Aniridia is a genetic disorder predominantly affecting the eye, caused by PAX6 haploinsufficiency due to mutations in one allele. Patients present vision loss and, in some cases, other systemic abnormalities. Increasing the expression of PAX6 early in life could block the progression of the disease. Now, Rabiee *et al.* used a pharmacological approach in vitro and in a rodent model of Pax6 haploinsufficiency (Pax6 $^{+/-}$). Through chemical screening, the authors showed that MEK inhibitors could increase PAX6 expression in corneal cells. Treating Pax6 $^{+/-}$ mice early in life with the inhibitor reduced eye abnormalities, suggesting that MEK inhibitors might be effective for treating postnatal abnormalities in patients with PAX6 haploinsufficiency.